Extremely low-noise avalanche photodiodes based on $AlAs_{0.56}Sb_{0.44}$

Xin Yi[a,d], Shiyu Xie[b], Baolai Liang[c], Leh W. Lim[a], Diana L. Huffaker[c], Chee H. Tan[a] and John P.R. David [a]*

[a]Department of Electronic and Electrical Engineering, University of Sheffield, Sheffield, S1 3JD, UK;
[b]School of Physics and Astronomy, Cardiff University, Cardiff, CF24 3AA, UK;
[c]California NanoSystems Institute, University of California-Los Angeles, Los Angeles, CA, USA;
[d]Current address: Institute of Photonics and Quantum Sciences, School of Engineering and Physical Sciences, Heriot-Watt University
* Email: j.p.david@sheffield.ac.uk

ABSTRACT

This paper presents the electron and hole avalanche multiplication and excess noise characteristics based on bulk $AlAs_{0.56}Sb_{0.44}$ p-i-n and n-i-p homojunction diodes lattice matched to InP, with nominal avalanche region thicknesses of 0.6 -1.5 µm. From these, the bulk electron and hole impact ionization coefficients (α and β respectively), have been determined over an electric field range of 220-1250 kV/cm for α and from 360-1250 kV/cm for β for the first time. Excess noise characteristics suggest an β/α ratio as low as 0.005 for an avalanche region of 1.5 µm in this material, close to the theoretical minimum and significantly lower than AlInAs, InP, or even silicon. This material can be easily integrated with InGaAs for networking and sensing applications, with modeling suggesting that a sensitivity of -32.1 dBm at a bit-error rate (BER) of 1×10^{-12} at 10 Gb/s at 1550 nm can be realized. This sensitivity can be improved even further by optimizing the dark currents and by using a lower noise transimpedance amplifier.

Keywords: Impact ionization, Avalanche photodiode, Avalanche multiplication, AlAsSb.

1. INTRODUCTION

Most telecommunication based systems utilizing fibre optic cables for the transmission of the light use InGaAs based detectors, as the attenuation minima in optical fibres is in the 1500-1650 nm wavelength range. Conventional InGaAs pin-diode detectors are capable of high-speed operation but their sensitivity is limited by the noise performance of the electronic amplifiers that are used. One way to overcome this limitation is to use avalanche photodiodes (APDs) which amplify the photogenerated current within the photodetector by utilizing the impact ionization process. For impact ionization to occur, the device has to operate at a relatively high electric field but due to the narrow bandgap of InGaAs (0.75 eV), this gives rise to large tunneling dark currents. To overcome this problem, modern APDs utilize a low electric field absorber region that comprises a thick layer of InGaAs to absorb the photons and a wider bandgap region where the impact ionization and carrier multiplication occurs – the so called Separate Absorption and Multiplication APD (SAM-APD) [1].

A major problem with SAM-APDs is that while we would like to operate the device at as high a multiplication value as possible, the impact ionization process which gives rise to the multiplication incurs a penalty. Both electrons and holes can ionize at high electric fields and these ionization coefficients (α for electrons and β for holes) are stochastic processes that are functions of the electric field. McIntyre [2] showed that there is an associated 'excess noise' in addition to the multiplied photocurrent shot noise term and that this is a function of the β/α ratio (or k). For low excess noise at high values of electron initiated multiplication (M_e), a small k is desirable as given by the expression for excess noise;

$$F_e = kM_e + (1-k)(2 - 1/M_e)$$

If the α and β are similar in value, the material will have a k value close to 1, and this means that as M_e increases, so does F_e. An ideal semiconductor avalanching material would have $k = 0$ in which case F_e would have a maximum value of 2. Another problem with using SAM-APDs is that they suffer from a reduction in speed at high multiplication, as multiple transits of the multiplication region may be required [3]. This depends on the β/α ratio as well and again, a smaller k (for

electron-initiated multiplication) is what is required for a high gain-bandwidth product (GBP) in a SAM-APD. High-speed SAM-APDs therefore tend to have thinner multiplication regions and consequently have to operate at higher electric fields. The α and β are material dependent parameters and Fig. 1 shows how these vary for a number of common semiconductor materials as a function of inverse electric field. The most common materials used for the multiplication region in telecommunication based SAM-APDs are InP and AlInAs as these are lattice matched to the InGaAs absorber region. From Fig. 1 we can see that the β/α ratio is broadly similar in both these materials, especially at the higher electric fields that high-speed SAM-APDs operate at. (Note that in InP, β is > α, so holes are used to initiate the multiplication process.) Such devices have their maximum useful multiplication limited by the onset of large 'excess noise' after which the overall sensitivity starts to decrease [4]. The ionization coefficients in a semiconductor are determined by the details of their band structure and there have been numerous attempts over the years to overcome these limitations by artificially modifying or 'engineering' their band-structure. Several groups have looked at using multiple quantum wells (MQWs) with the thinking being that electrons will gain more energy by falling from the barrier into the quantum well than a hole would (due to the different band discontinuities), thereby enhancing the β/α ratio [5-7]. Other groups have looked at using nanowires [8] and quantum dots [9,10] as means for enhancing the β/α ratio. Recently, some groups have used a Ge absorber grown on a silicon multiplication region as a way to achieve a small β/α ratio at 1310 nm [11]. While some of these attempts have managed to give rise to improvements in the β/α ratio, it has involved complicated growth and processing technologies. Some narrow bandgap semiconductors like InAs [12] and HgCdTe [13] appear to naturally possess a vanishingly small β/α ratio – the so called e-APDs. Due to the small bandgap in these materials (E_g ~ 0.25-0.4 eV), the electrons ionize at relatively low electric fields before they scatter into the satellite valleys of the conduction band. Unfortunately, this small bandgap means room temperature operation of these devices is not possible and some form of cooling is required to reduce their dark currents. Recently, Campbell et al. [14,15] showed that the AlInAsSb alloy had a small β/α ratio and excess noise that was comparable to, or superior to that of silicon. This material has a large bandgap of 1.24 eV and can operate at room temperature, however it has to be grown lattice matched on GaSb substrates. In this paper, we report on the ionization coefficients and excess noise in another alloy system that contains Sb, namely AlAsSb, and that has the advantage of being lattice matched to InGaAs and InP. We show that this alloy possesses a very small β/α value at low electric fields and is potentially capable of operating with high multiplication and at very high speeds. Early work on AlAsSb was undertaken on extremely thin avalanching structures and while good multiplication characteristics could be obtained, the excess noise was found to increase linearly as the multiplication increased, suggesting that β/α ~ 1 and the relatively low noise seen was due to dead-space effects [16].

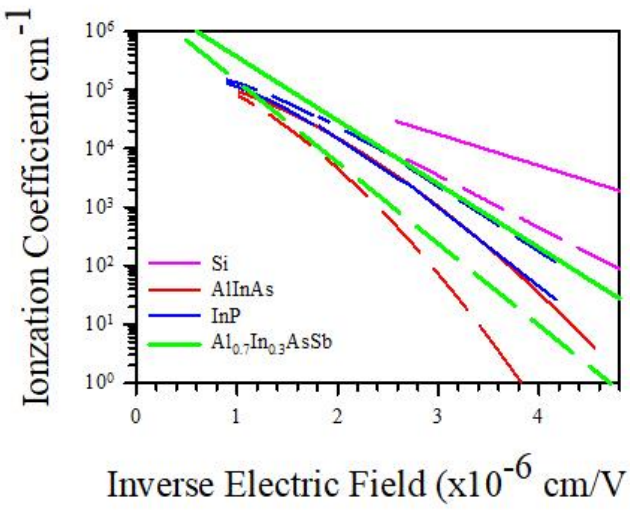

Fig 1. Ionization coefficients as a function of inverse electric field for InP [17], AlInAs [18], silicon [19] and $Al_{0.7}In_{0.3}AsSb$ [15]. Both silicon and $Al_{0.7}In_{0.3}AsSb$ have better k values than InP or AlInAs, especially at the lower electric fields.

2. RESULTS

2.1 Device growth and fabrication

The AlAsSb p-i-n and n-i-p structures used in this study were grown on epi-ready n-InP (001) and p-InP (001) substrates respectively, via a digital alloy growth technology in a Veeco GEN930 MBE reactor, in which both As_2 and Sb_2 fluxes are supplied using valved cracker cells [20]. The challenge here was to grow a thick ternary random alloy with two group V elements (As and Sb). The Sb/As composition is extremely sensitive to the growth conditions and small changes to substrate or source temperatures can cause thick structures to be mismatched. Growing AlSb/AlAs as a digital alloy gave much more controllable growth. The digital AlAsSb layer was realised by periodically alternating the As_2 and Sb_2 shutter while maintaining a steady Al flux during deposition, resulting in AlSb and AlAs equivalent sequence of 4.0 and 0.44 monolayers. The layers grown include five homojunction p-i-n (n-i-p) structures (the structures are labelled P1-P3 and N1-N2 for easy reference and are detailed in Table 1). The nominal multiplication region thicknesses are w = 1.5, 1.0 and 0.6 μm, respectively. The multiplication region is sandwiched between a top 300-nm p^+/n^+ AlAsSb and a bottom 100-nm p^+/n^+ AlAsSb cladding layers with Be(p^+) and Te(n^+) doping concentrations of 2.0×10^{18} cm^{-3}. The structure also has a highly doped (1.0×10^{19} cm^{-3}) top 20-nm and bottom 500-nm InGaAs contact layers. Fig.2a shows an example of the X-ray diffraction (XRD) results obtained on P1, with 1900 nm of AlAsSb. The clear peaks and pendellösung fringes show that the InGaAs and AlAsSb are reasonably lattice-matched to the InP substrate. All the samples had a mirror surface with no evidence of cross-hatching. The top thin InGaAs cap prevents oxidation of AlAsSb and also helps form a good ohmic metal contact (see Fig. 2b). Mesa devices were fabricated using conventional wet chemical etching but were not optimized for low dark current or passivated. All devices investigated showed good diode characteristics with forward ideality factors of ~2 (up to forward currents of 0.1mA) and low enough reverse dark currents to enable us to determine the photomultiplication characteristics until the device breakdown voltage (Fig. 3a). Capacitance-voltage (CV) measurements showed that the background doping was typically between 5-10×10^{15} cm^{-3} and approximately -8 V was required to fully deplete the 0.6 μm structure [21]. The spectral response of the devices as a function of wavelength were obtained using a lamp and monochromator system. This was done under different reverse bias conditions and Fig. 3b shows the measured spectral response for P2. The red symbols show the ratio of the photocurrent between -35 V and -8 V. The increase of photocurrent seen at low biases at the shorter wavelengths (from 0 V to -8 V) is due to the increasing depletion width in the p-type intrinsic region. This behaviour suggests that the electron diffusion length in the undepleted p-type intrinsic regions is relatively short and has been estimated to be typically about 70nm. The red symbols in Fig. 3b show that the photocurrent increases more rapidly at shorter wavelengths beyond -8V, suggesting that the α is significantly larger than β.

Table 1. Layer details of the five AlAsSb layers grown.

Layer name	Diode type	Nominal i-thickness (μm)	i-region doping from CV (×10^{15} cm^{-3}) p-type	i-region thickness from CV (μm)
P1	p-i-n	1.5	5	1.55
P2	p-i-n	0.6	10	0.66
P3	p-i-n	1.0	10	1.15
N1	n-i-p	1.5	5	1.55
N2	n-i-p	0.6	10	0.66

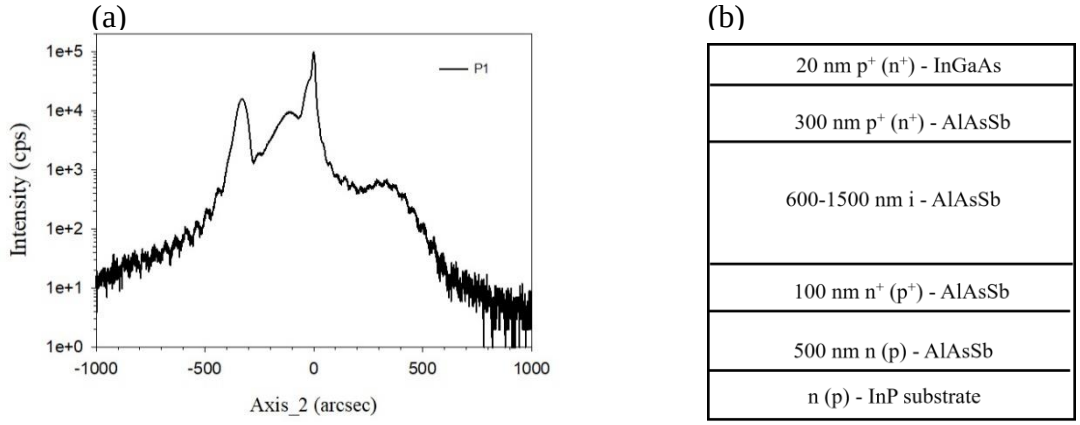

Fig 2. (a) The x-ray rocking curve of the 1.5 µm thick p-i-n (P1). The mismatch of the digital alloy is relatively small, considering the total thickness of the AlAsSb layer grown (b) A schematic diagram of the nominal p-i-n (n-i-p) structues grown.

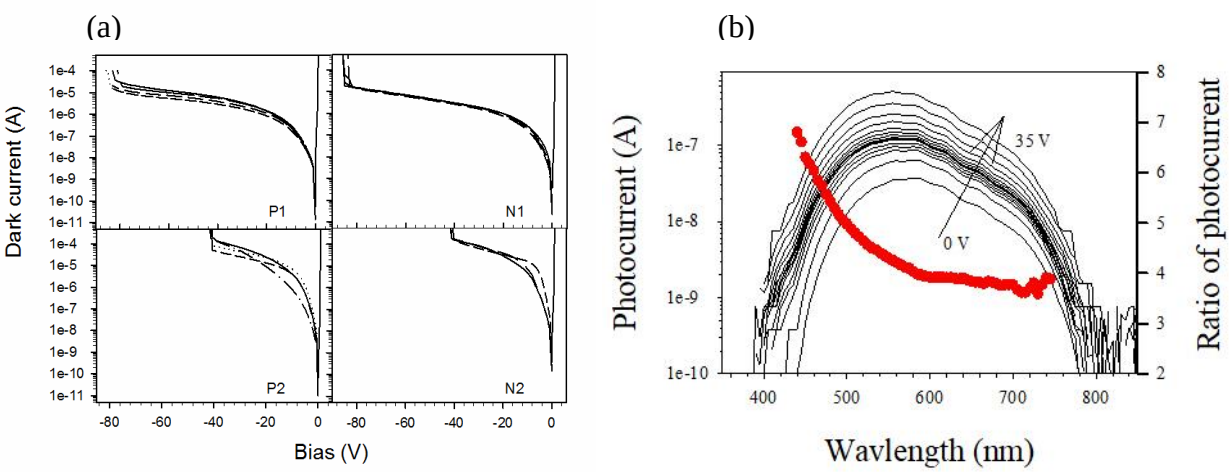

Fig. 3. (a) Room temperature forward and reverse dark currents. The initial rapid increase in reverse dark current suggests that the unpassivated devices have a large surface dark current component. (b) Bias dependent photocurrent for P2. The initial increase in photocurrent from 0 V to -8 V is due to the movement of the depletion edge. Beyond -8 V, the increasing photocurrent is due to the onset of avalanche multiplication. The red symbols show the ratio of the increase in photocurrent between -35 V and -8 V.

2.2 Impact ionization coefficients

The electron and hole initiated photomultiplication characteristics (M_e and M_h respectively) were done using 405 nm illumination on the p-i-n and n-i-p structures. Several devices from each layer were measured and different illumination powers were used to ensure the reproducibility of the results. At this wavelength, almost all the light is absorbed in the top 300 nm doped cladding regions, ensuring that the multiplication is initiated by only minority electrons or holes that diffuse into the high field region. Due to the non-negligible p-type background doping in the intrinsic region and the short electron diffusion lengths, the M_e measurements showed a significant increase in photocurrent even at low reverse biases that was not due to the onset of impact ionization but the movement of the depletion edge [22]. All the photocurrent measurements were corrected for this effect. AlAsSb is an indirect bandgap material so using 633 nm illumination results in light that is only weakly absorbed by the structure and consequently we can assume a uniform generation rate of carriers throughout

the multiplication region. Fig. 4a shows the measured bias dependent photocurrent on P1 and N1 with illumination of 405 nm and 633 nm wavelength light. P1 (P2) and N1 (N2) have similar intrinsic thicknesses but the shape of the photocurrent with 405 nm wavelength illumination is significantly different, with the onset of multiplication occurring at a much lower voltage in the p-i-n structures, and this difference is more obvious in the P1-N1 pair due to their much thicker intrinsic region. M_h from N1 did not show any appreciable increase with reverse bias until you approached the breakdown voltage. However, when 633-nm wavelength illumination is used, the shape of the multiplication versus voltage characteristic is very similar in both structures as the carriers initiating the multiplication are uniformly generated across the structure. This large difference in M_e and M_h is extremely significant and suggests that the β/α ratio in AlAsSb is very small. The α and β were extracted from the multiplication characteristics assuming a tapered electric field in the devices and no 'dead-space' effects [23]. Measurements on much thinner AlAsSb p-i-ns [16] were also used to extract the ionization coefficients at the very high fields where the β/α ratio is close to 1. These ionization coefficients are shown graphically in Fig. 4b, together with the β/α ratio as a function of inverse electric field. This shows that a β/α ratio of <0.01 can be achieved at electric fields below 460 kV/cm and this ratio can be even potentially <0.001 at electric fields below 360 kV/cm. These coefficients are capable of reproducing the measured M_e and M_h for the different avalanche layer structures accurately over a wide range of multiplication values.

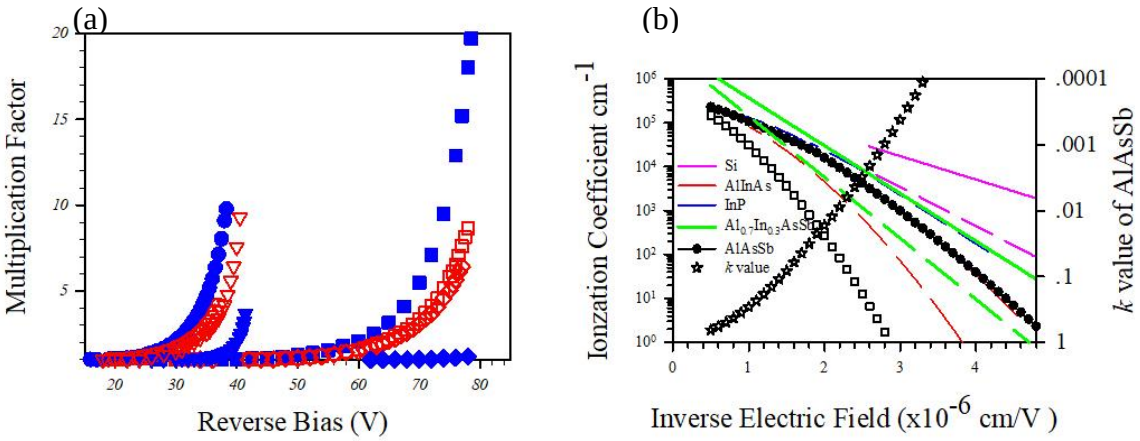

Fig. 4. (a) M_e and M_h (405 nm illumination) on P1/N1 and P2/N2 which are significantly different (blue symbols). The red symbols show the multiplication with 633 nm illumination which is similar for each p-i-n and n-i-p pair. (b) The α (circle) and β (square) extracted from the multiplication characteristics in AlAsSb, compared to other materials and silicon. Solid lines represent α and dashed lines represent β. The k value (β/α) (star) is extremely small at lower electric fields but approaches unity as the electric field approaches 1 MV/cm.

2.3 Excess noise

To achieve low excess noise in AlAsSb, electrons have to initiate the multiplication. Measurements of the excess noise were undertaken using the system as described by Lau et al [24]. This uses a transimpedance amplifier (TIA) front end and has a phase sensitive measurement system that removes the contribution from any dark currents. This allows us to accurately measure the noise at high values of gain, even in the presence of large dark currents. Fig. 5a shows the excess noise due to electron-initiated multiplication, F_e, for P1, P2 and P3, as well as the theoretical values predicted by the McIntyre equation for different values of k. Only the presence of edge breakdown due to non-optimised device fabrication prevented measurements at even higher multiplication values. Layers P1 and P3 show very low excess noise (F_e) corresponding to effective k values of 0.005 and 0.012 respectively. P2 demonstrates a larger effective k of 0.04 due to the higher electric field encountered in the thinner avalanching region and hence larger β/α, however even this is still significantly better than the excess noise seen in InP, InAlAs or silicon. To demonstrate that the very low excess noise seen in P1-P3 in Fig. 3b is due to the large asymmetry in α and β, Fig. 5b show measurements undertaken on P1 with longer wavelength light of 543 nm and 633 nm, where carriers initiating the avalanche process are increasingly created deeper within the avalanche multiplication region. The fraction of holes contributing to the multiplication process increases as the wavelength increases in the p-i-n structure, and as expected, the excess noise also increases, with the opposite trend seen in the n-i-p structure. No F_h measurements could be undertaken on n-i-p structures as the bias voltage when

appreciable multiplication occurs was very close to the device breakdown voltage, however measurements using 543 nm which is largely hole initiated multiplication shows a very high excess noise. This noise value reduces significantly with 633 nm illumination. Note that the 633nm illumination in P1 still manages to have a relatively low $F = 3$ at M~20 despite having both electrons and holes initiating the multiplication process. Under such 'mixed' carrier injection conditions, the F does not follow the theoretical McIntyre expression given earlier which is only valid for single carrier injection into an avalanching region. Although the effect of such mixed carrier generation on the excess noise has been looked at by others [24], it has been only in materials where the k was close to 1, and as such no significant changes in the excess noise were observed with the wavelength used. Recently, Hossain et al. [26] reported an exact analytical formulation for mixed carrier injection, taking into account the photon absorption profile within the avalanching region of an APD. Providing the absorption profile of the different wavelengths of light contributing to the overall multiplication process was accurately known, this technique allows the associated excess noise to be calculated accurately. Fig. 5b also presents the simulated excess noise results on P1 assuming light is absorbed with different absorption coefficients using this model within the avalanching region, with no contribution from the doped cladding regions. The blue, green and red circles show the measured excess noise from P1 using 420 nm, 543 nm and 633 nm wavelengths of illumination respectively. The dark blue line shows the modelled excess noise with almost pure electron-initiated multiplication while the green line shows the result for a slightly more 'mixed' case. The red line is what we would expect if we had electrons and holes being created uniformly across the multiplication region. This explains qualitatively the trends that we see experimentally but the discrepancy seen with 633 nm illumination may be due to an underestimate of the photocurrent contributed by the p^+ region. Fig. 5c shows that the F_e results at $M = 10$ in these AlAsSb structures, compared with other materials such as Si [27], AlInAs [28] and AlInAsSb [14]. Only InAs [29] appears capable of giving a significantly lower value of excess noise.

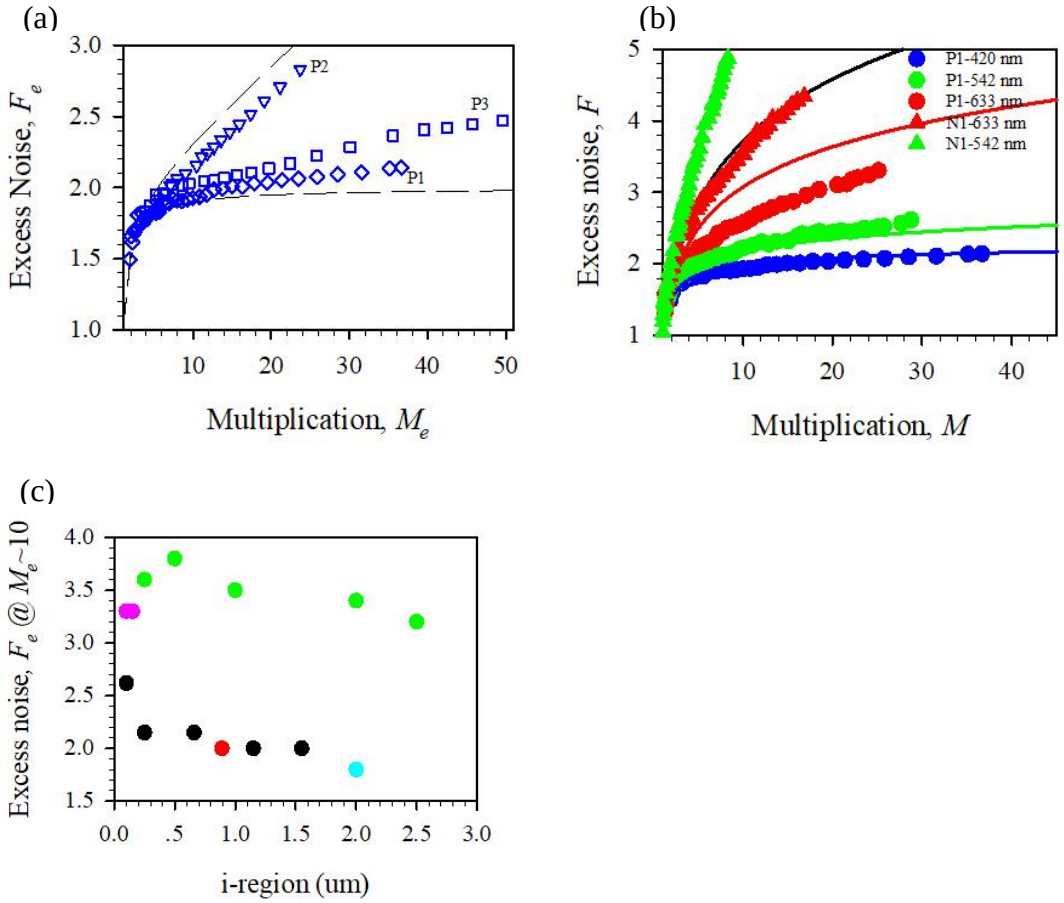

Fig. 5. (a) Measured F_e in P1-P3. The dashed black lines show the ideal McIntyre excess noise curve for different k increasing from 0 in steps of 0.05. (b) The measured excess noise (symbols) from P1 and N1 using different wavelength light. Solid lines are simulated excess noise as described in the text. (c) The excess noise comparision at a multiplication of 10 for different thickness avalanching materials as follows: AlInAs (green), silicon (pink), AlInAsSb (red) InAs (cyan) and AlAsSb (black).

2.4 Sensitivity analysis

We previously modelled the performance of 30 μm diameter InGaAs-AlAsSb based SAM-APDs [30] where we showed that it was possible to achieve a sensitivity of -32.1 dBm at BER=10^{-12} at 1550 nm for a 10 Gb/s optical system. The prediction there assumed an InGaAs absorption region that is 600 nm thick with a maximized-induced current (MIC) design [31] and capable of a unity gain responsivity of 0.92 A/W. Fig. 5a shows how the sensitivity initially increases with the gain but then saturates for devices with 1000 nm thick (for 10 Gb/s) and 1500 nm thick (for 2.5 Gb/s) multiplication regions. The device performance here is limited by the device surface dark current and the noise of commercially available TIAs (6.6 pA $Hz^{-1/2}$ for 2.5 Gb/s and 11 pA $Hz^{-1/2}$ for 10 Gb/s), rather than factors such as the avalanche build-up time or the excess noise factor. Surface dark currents of 1.75 μA and bulk dark currents of 16 nA were assumed in this analysis. The impact ionization process in the multiplication region was simulated using a Random Path Length (RPL) model [32]. This enables us to extract the mean current impulse for different values of multiplication, which was then Fourier Transformed to give the -3dB point as the bandwidth. Fig. 5b shows the sensitivity that is achievable at 2.5 Gb/s and 10 Gb/s for the best experimentally reported Si/Ge and AlInAs based devices as well as the predicted results for AlAsSb from Fig. 5a. Our new simulations show that if the device surface currents could be reduced by optimized etching and passivation techniques, such that the device surface current is 500 nA, bulk dark current at unity gain is only 1 pA and we used

commercial available TIAs, we can get improved sensitivities of -39.9 dBm and -34.7 dBm. To take full advantage of the potential performance of AlAsSb SAM-APDs, not only will the surface dark currents have to be further reduced, the TIA noise will also have to be reduced.

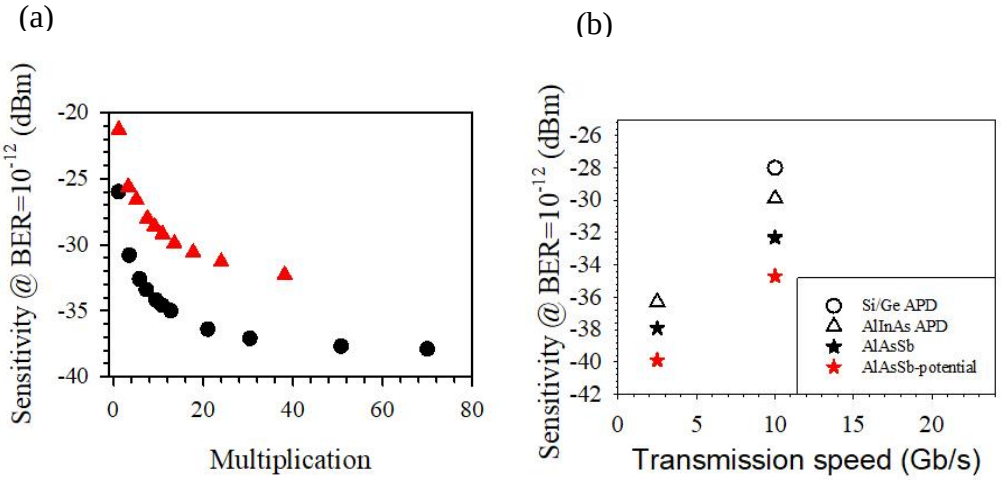

Fig. 6. (a) Sensitivity versus multiplication calculated for 1000nm thick (red symbols) and 1500nm thick (black symbols) avalanche width SAM-APDs. A 600nm InGaAs absorber was assumed with realistic dark currents and TIA noise. (b) The best reported sensitivities from competing technologies in the literature and the potential performance of AlAsSb based SAM-APDs.

3. DISCUSSION AND CONCLUSION

Measurements of the impact ionization coefficients and the excess noise suggest that AlAsSb has the smallest β/α ratio of any wide bandgap III-V semiconductor to date, and the fact that it can be grown lattice matched to InP makes it an ideal candidate for the low level detection of 1550 nm photons. This small β/α ratio has the added benefit that it will enable wider multiplication regions to be utilized, without paying a penalty in terms of the speed or GBP. As the β/α ratio in this material tends towards 1 as the electric field increases, it will be hard to avoid multiplication regions that are thinner than 1000 nm while maintaining its low excess noise properties, and this will necessitate the use of high voltages. Nevertheless the AlAsSb alloy system offers the potential for extremely high sensitivity 1550 nm detectors. One problem encountered with AlAsSb is that the material system is prone to oxidizing very easily when exposed to air, consequently passivation of the devices is necessary. Excess noise measurements on thin AlGaAsSb (Al=85%) p-i-n diodes showed that a $k = 0.1$ could be achieved with a 87 nm avalanching width and that this improved to $k = 0.05$ when the width increased to 170 nm [33]. A much thicker structure may well give similar k values to that seen in AlAsSb, but with the added advantage that the AlGaAsSb material system should be more stable.

ACKNOWLEDGEMENTS

D.L.H. acknowledges financial support provided by the Sêr Cymru National Research Network in Advanced Engineering and Materials. S.Y.X. acknowledges financial support from the European Regional Development Fund through the Welsh Government. B.L.L. acknowledges support from the National Science Foundation of the United States (ECCS-1810507).

REFERENCES

[1] Campbell., J. C. et al. Recent advances in avalanche photodiodes. IEEE J. Sel. Topics Quantum Electron. **10**, 777–787 (2004).

[2] McIntyre, R. J. Multiplication noise in uniform avalanche diodes. IEEE Transactions Electron Devices. **ED 13**, 164–168 (1966).

[3] Emmons, R.B. Avalanche photodiodes frequency response. J. Appl. Phys. **38**, 3705 (1967).

[4] Agrawal, G. P. in Fiber-Optic Communication Systems 3rd edn, Ch. 4 (Wiley, 2002).

[5] Capasso, F. Tsang, W. & Williams, G. F. Staircase solid-state photomultipliers and avalanche photodiodes with enhanced ionization rates ratio. IEEE Tans. Electron Devices **30**, 381-390 (1982).

[6] Ren, M. *et al.* AlInAsSb/GaSb staircase avalanche photodiode. *Applied Physics Letters* **108,** 081101 (2016).

[7] Wang, S. et al. Low-noise impact-ionization-engineered avalanche photodiodes grown on InP substrates. IEEE Photonics Tech. Lett. **14**, 1722-1724 (2002).

[8] Farrell, A.C. et al. Plasmonic field confinement for separate absorption-multiplication in InGaAs nanopillar avalanche photodiodes. Sci. Rep. **5**, 17580 (2015).

[9] Chen, B. *et al.* Low Dark Current High Gain InAs Quantum Dot Avalanche Photodiodes Monolithically Grown on Si. *ACS Photonics* **7,** 528–533 (2020).

[10] Ma, Y. et al. Enhanced carrier multiplication in InAs quantum dots for bulk avalanche photodetector applications. Adv. optical mater. **5**, 1601023 (2017).

[11] Peter, V. et al. High performance planar germanium-on0silicon single-photon avalanche diode detectors. Nat. Comm. **10**, 1089 (2019).

[12] Marshall, A.R.J., Ker, P.J., Krysa, A., David, J.P.R. & Tan, C.H. High speed InAs electron avalanche photodiodes overcome the conventional gain-bandwidth product limit. Opt. Express. **23**, 23341-23349 (2011).

[13] Beck J.D. Wan Changfeng, Kinch M.A., Robinson J.E. MWIR HgCdTe avalanche photodiode. Proc. SPIE 4454, Material for infrared detectors (2001).

[14] Bank., S. R. et al. Avalanche Photodiodes Based on the AlInAsSb Materials System. IEEE Journal of Selected Topics in Quantum Electronics **24**, 1–7 (2018).

[15] Yuan, Y. et al. AlInAsSb impact ionization coefficients. IEEE Photon.Tech. Let. **31**, 315-318 (2019).

[16] Xie, J. et al. Excess noise characteristics of thin AlAsSb APDs. IEEE transactions on electron devices. **59**, 1475-1479 (2012).

[17] Cook, L. W., Bulman, G. E. & Stillman, G. E. Electron and hole impact ionization coefficients in InP determined by photomultiplication measurements. App. Phys. Lett. 40, 589–591 (1982).

[18] Goh, Y. L. et al. Avalanche Multiplication in InAlAs. IEEE Transactions on Electron Devices. **54**, 11–16 (2007).

[19] Van, Overstraeten, R. & Man, H. D. Measurement of the ionization rates in diffused silicon p-n junctions. Solid-State Electron. 13, 583–608 (1970).

[20] Juang. B, et al. Optical characterization of AlAsSb digital alloy and random alloy on GaSb. Crystals. **7**, 213 (1017).

[21] Yi, X. et al. Demonstration of large ionization coefficient ratio in AlAsSb lattice matched to InP. Scientific Reports. **8**, 9107 (2018).

[22] Woods, M. H., Johnson, W. C. & Lambert, M. A. Use of a Schottky barrier to measure impact ionization coefficients in semiconductors. *Solid State Electron.* **16**, 381–394 (1973).

[23] Grant, W. N. Electron and hole ionization rates in epitaxial silicon at high electric fields. Solid-state Electronics. **16**, 1189–1203 (1973).

[24] Lau, K. S. et al. Excess noise measurement in avalanche photodiodes using a transimpedance amplifier front-end. Measurement science and technology. **17**, (2006).

[25] Li, F. K. et al. Avalanche noise characteristics of thin GaAs structures with distributed carrier generation. IEEE transactions on electron devices. **47**, 910-914 (2000).

[26] Md, Mottaleb Hossain, John P. R. David, and Majeed M. Hayat. Exact Analytical Formula for the Excess Noise Factor for Mixed Carrier Injection Avalanche Photodiodes. J. Lightwave Technol. **37**, 3315-3323 (2019).

[27] C. H. Tan, J. C. Clark, J. P. R. David, G. J. Rees, S. A. Plimmer, R. C. Tozer, et al. Avalanche noise measurement in thin Si p^+-i-n^+ diodes. Applied Physics Letters, **76**, 3926-3928 (2000).

[28] Y. L. Goh, A. R. J. Marshall, D. J. Massey, J. S. Ng, C. H. Tan, M. Hopkinson, et al. Excess Avalanche Noise in $In_{0.52}Al_{0.48}As$, IEEE Journal of Quantum Electronics, **43**, 503-507 (2007).

[29] A.R.J. Marshall, C.H. Tan, M. J. Steer, and J.P.R. David, Extremely low excess noise in InAs electron avalanche photodiodes, IEEE Photon. Tech. Lett., **21**, 13 (2009).
[30] Yi, X. et al. Extremely low excess noise and high sensitivity AlAsSb avalanche photodiode. Nature Photonics. **13**, 683-686 (2019).
[31] Nada, M. et al. 50-Gbit/s vertical illumination avalanche photodiode for 400-Gbit/s ethernet systems. Opt. Express. **22**, 14681–14687 (2014).
[32] Ong, D. S. et al. A simple model to determine multiplication and noise in avalanche photodiodes. J. Appl. Phys. **83**, 3426 (1998).
[33] Pinel, L. et al. Effect of carrier injection profile on low noise thin $Al_{0.85}Ga_{0.15}AsSb$ avalanche photodiodes. Optics Express. **26**, 3568-3576 (2018).